Available online at www.sciencedirect.com
SCIENCE DIRECT®
Journal of Catalysis 227 (2004) 26–32
JOURNAL OF CATALYSIS
www.elsevier.com/locate/jcat

Porous anodic alumina optimized as a catalyst support for microreactors

J.C. Ganley, K.L. Riechmann, E.G. Seebauer, R.I. Masel *

Department of Chemical and Biomolecular Engineering, University of Illinois at Urbana-Champaign, 213 Roger Adams Laboratory, Box C-3, 600 S. Mathews Avenue, Urbana, IL 61801-3792, USA

Received 15 April 2004; revised 24 May 2004; accepted 15 June 2004

Available online 20 July 2004

Abstract

This paper describes the optimization of process conditions for making porous anodic alumina as a catalyst support in monolithic microreactors. The basic process involves direct current anodization of 1100 alloy aluminum in oxalic acid. Electrolyte concentration, temperature, and anodization potential are optimized with respect to oxidation efficiency and pore density via a Box–Behnken experimental design to the values of 0.6 M, 18 °C, and 30 V, respectively. The effects of subsequent hydrothermal–thermal treatment on the surface area enhancement and surface morphology of the porous oxide are also investigated and optimized. The resulting films are employed in the fabrication of active catalytic aluminum–alumina microreactors for the decomposition of ammonia to hydrogen and nitrogen.

Keywords: Anodic alumina catalyst support; Surface area optimization; Ammonia reforming

1. Introduction

The anodic oxidation of aluminum surfaces to form overlaying films of porous aluminum oxide, also known as alumite, is a common process employed in the metal finishing industry as a first step to passivate and protect aluminum surfaces from corrosion and abrasion. Under appropriate conditions on properly prepared substrates, a regular array of nanometer-scale pores can be formed [1–3]. This structure lends itself to a wide range of applications, including forms for electroplating metal nanowires [4–6], templates for the creation of carbon [7,8] or titanium dioxide [9,10] nanotubes, and catalysts or catalyst supports [11–14]. This last set of applications concerns the present work.

Anodic films can serve as effective catalysts or catalyst supports within microreactors for several reasons. The films may be grown to thicknesses over a hundred micrometers [15,16] and exhibit significant specific surface areas (typically 10–40 m^2/g) [12,14]. Thus, substantial total surface areas may be conformally located within confined microreactor geometries. Furthermore, the films offer very little resistance to diffusive mass transfer, particularly compared to extruded or sol-derived alumina [11]. Note, however, that the specific surface area of anodic alumina lies far below that of traditional alumina powders or pellets. Other attractive properties of anodized films include strong adhesion to the substrate and nontrivial hardness [17,18].

Previous work from this laboratory has demonstrated the use of anodized alumina in the context of microreactors for ammonia decomposition [19]. However, the synthesis procedure reported in that work yields films only 60 μm thick with specific surface areas near 16 m^2/g. Commercially viable microreactors require thicker films and higher specific surface areas, however. The present work develops optimized procedures for accomplishing these increases—to yield films from 50 to 90 μm thick with specific areas of over 150 m^2/g. In addition, this work demonstrates a hydrothermal treatment method for anodized films that boosts their specific surface areas by a factor of 10. When the alumina is used to support metal catalysts such as Ru or Ni, this treatment increases the catalyst dispersion by factors around 2 to 3.

* Corresponding author.
E-mail address: r-masel@uiuc.edu (R.I. Masel).

0021-9517/$ – see front matter
doi:10.1016/j.jcat.2004.06.016

2. Methodological background

2.1. Optimization of anodization conditions

Many previous experimental and modeling studies have investigated the phenomenology and mechanisms by which anodic alumina grows and develops. Key process variables include the temperature of the electrolyte, the anodization potential or current density, and the pH or concentration of the electrolyte [2,14,15,20–22]. The present work employs a Box–Behnken design [23] with these variables to maximize the pore density and the oxidation efficiency by which the anodic layers form. This statistical experimental design method applies to a wide range of experimental systems [24–26] and generates a full quadratic empirical model between variables and experimental responses.

2.2. Treatment of anodized films

A porous anodic oxide created for decoration or corrosion protection is typically sealed after formation by treatment in hot water or steam [27]. Hydration and expansion of the aluminum oxide cause the nanopores to close. Although the exact nature of the hydrated oxide is not known, it is believed to contain boehmite [28], psuedoboehmite [29], and physically adsorbed water [27]. Hydrothermal treatment of α-alumina has been shown to produce surface gibbsite–bayerite [30].

Importantly for the present work, the hydrated alumina hydroxides boehmite, gibbsite, and bayerite may be converted upon dehydration to the high-surface area δ- or γ-alumina phases under the proper conditions [31]. Correspondingly, dehydration of sealed porous alumina films causes a significant increase in specific and total oxide surface area; however, some oxide is lost with successive treatments after the first [32]. This study subjects anodized alumina in a microreactor configuration to hydrothermal–thermal treatments to determine the suitability of this approach as a fabrication technique. Process conditions are adjusted to yield the highest surface area of alumina, and the effects of this procedure on the dispersion of several metal catalysts supported by the alumina are examined.

3. Experimental

3.1. Anodization optimization

Box–Behnken optimization of anodization process conditions was carried out by varying the anodization potential as well as the temperature and concentration of aqueous oxalic acid solutions. Each factor was tested at a preselected low, moderate, or high value simultaneously with the other two factors as prescribed by a standard three-factor Box–Behnken experimental design [23–26]. Electrolyte temperature was set to 0, 10, or 25 °C. Other studies have shown that anodization processes carried out at higher temperatures dramatically decreases the oxide formation current efficiency, leading to severe aluminum dissolution [14,20,22]. The formation of porous anodic alumina films in oxalic acid electrolytes has been shown to be optimized between 30 and 60 V [4,21], and our laboratory studies show that aqueous oxalic acid solutions become saturated above about 0.6 M at low (near 0 °C) temperatures. Therefore, anodization potential was set to 30, 45, or 60 V; and oxalic acid concentrations were 0.20, 0.40, and 0.60 M.

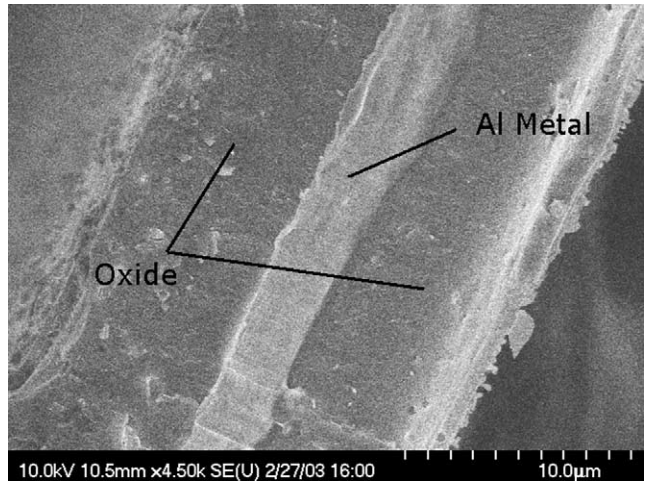

Fig. 1. Typical cross section of anodized 1100 alloy aluminum shim.

Sheets of 1100 aluminum alloy shim (ShopAid, Inc.) were used as substrates. 1100 Al is a high-purity aluminum alloy (minimum 99% Al, 0.65% Si and Fe, 0.1% Zn, 0.05% Mn, 0.05% Cu, 0.15% other). All samples were first degreased in acetone, and then anodized for 30 min at the appropriate process conditions to be tested. The thin anodic film was then removed by immersion in a 1.5 wt% chromic acid and 6 wt% phosphoric acid solution at 60 °C for 15 min [9]. Removal of this first anodic film allowed a second, thicker film to be grown on a surface free of the defects and surface scratches common to cold-worked aluminum foils. The samples were reanodized for 2 h and dried in a convection oven at 150 °C for 4 h. The anodized films were analyzed using high-resolution scanning electron microscopy (SEM, Hitachi S-4700). Plan-view images were used to determine pore density, and cross-sectional images yielded the thickness. A typical shim cross-section micrograph appears in Fig. 1.

3.2. Hydrothermal–thermal alumina treatment

Aluminum microreactors were constructed from rolled bar stock of 1100 aluminum (99+% Al). Electrical discharge machining (EDM) was employed to cut 14 parallel channels along the reactor's length. Each channel was 300 µm wide and 3 mm deep. The thickness of each wall separating two channels was 300 µm. Reactors were 9.2 mm wide, 12.6 mm long, and 4 mm thick. A photograph of a typical reactor is shown in Fig. 2. Using the optimum anodization conditions found using the above procedure (30 V, 18 °C, 0.6 M oxalic

Fig. 2. Photograph of an anodized channel microreactor beside a US penny.

acid), the reactors were anodized using the same two-step procedure outlined in the previous section. Some reactors were treated one or more times in the following manner: Immersion in deionized water at 100 °C for 1 h, drying in a convection oven at 150 °C for 30 min, and then dehydration at 550 °C in a tube furnace under air for 16 h.

The total surface area of each reactor was determined using single-point BET with a commercial unit (Micromeritics ChemiSorb 2705), with nitrogen physisorption at 77 K. The oxide pore structure was examined using high-resolution SEM (Hitachi S-4700). X-ray diffraction (Rigaku D-Max) was used to assess the oxide crystallinity. The total pore volume was estimated by the weighing the reactor before and after immersion in deionized water at room temperature.

3.3. Catalytic reactor tests

EDM-microstructured channel microreactors were anodized by the above two-step process under the conditions determined to be optimum as described above, with the second anodization step increased to 16 h to provide an oxide coating of at least 60 µm thickness. Some reactors were subjected to one hydrothermal–thermal treatment as outlined in Section 3.2. Metal catalyst was then deposited by wet impregnation with one of the following solutions: 0.20 M $RuCl_3$, 0.20 M $RhCl_3$, or 0.44 M $Ni(NO_3)_2$ in a solvent of 75% acetone and 25% water. This procedure provided for a catalyst loading of 1 wt% in each case. The reactors were dried in a convection oven at 150 °C for 1 h, calcined in a tube furnace under air for 4 h at 550 °C, and reduced in hydrogen at the same temperature. Active metal dispersion for each reactor was calculated using pulsed CO adsorption at room temperature in a commercial unit (Micromeritics ChemiSorb 2705), assuming a 1:1 ratio of adsorbed CO to exposed catalytic metal.

After each catalytic microreactor was prepared, reactivity was measured in a quartz tube heated by a temperature-controlled tube furnace. A few alumina pellets placed upstream of the reactor housing served as a reactant preheater. Concentrations in the product stream were monitored by passing all reactor effluent through an on-line thermal conductivity detector. The detector was calibrated by passing known mixtures of ammonia, hydrogen, and nitrogen through the reactor bypass. Control experiments throughout the temperature range of interest showed that the reactor housing induced no conversion in the absence of catalyst.

The reactant stream consisted of technical grade (99.99%) anhydrous ammonia flowing at 92 standard cubic centimeters per minute (sccm) and controlled with a calibrated mass-flow meter. All experiments were carried out at atmospheric pressure.

4. Results and discussion

4.1. Anodization optimization

Box–Behnken experiments showed that temperature exerted virtually no influence upon pore density. Thus, a response surface showing the influence of the two remaining variables (anodization potential and oxalic acid concentration) could be constructed in simple two-dimensional form. Fig. 3 shows this response surface using data taken at 10 °C. The strong dependence of pore density on anodization potential is apparent in the response surface. This behavior agrees with the observations of others who have attempted to "tune" pore diameter by adjusting either the anodization potential or the associated anodization current density [2,14,15,20–22]. The present work sought to obtain the highest density of pores possible, which occurred at the lowest anodization potential (30 V) and highest oxalic acid concentration (0.6 M) as the best process conditions.

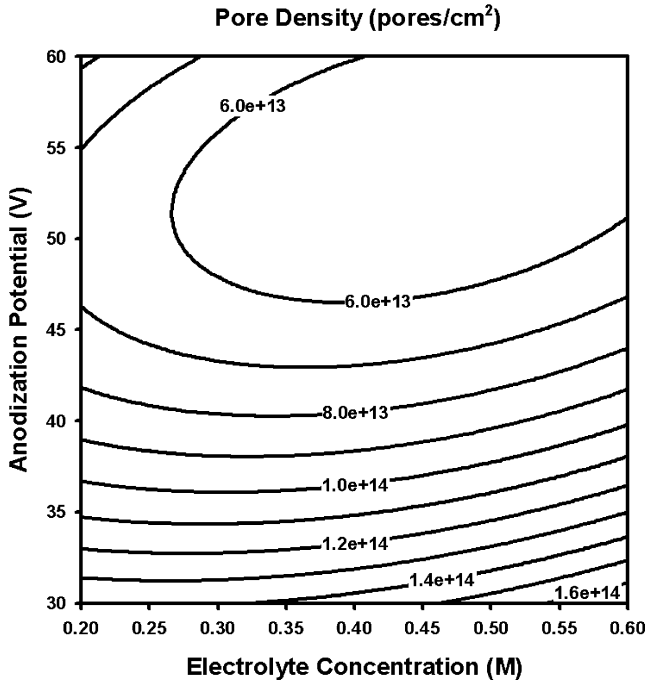

Fig. 3. Response surface plot of anodic oxide pore density as a function of oxalic acid concentration and anodization potential. Values shown correspond to an electrolyte temperature of 10 °C.

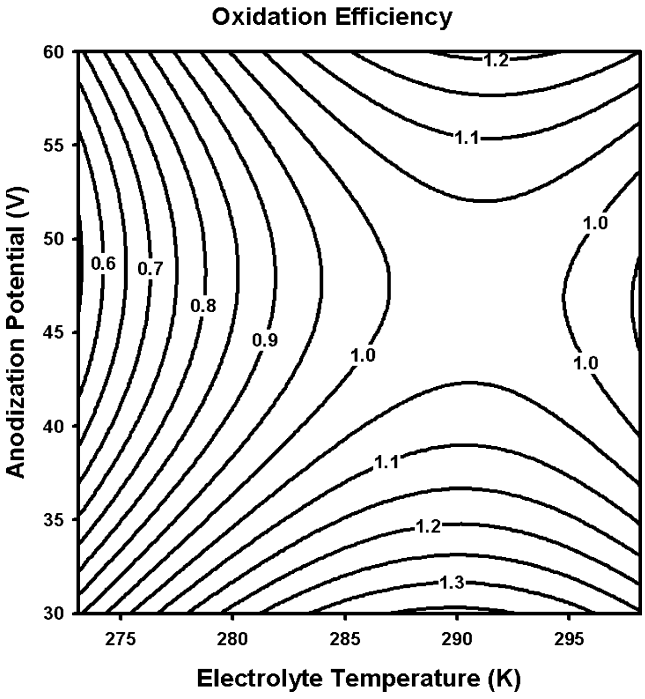

Fig. 4. Response surface plot of oxidation efficiency as a function of electrolyte temperature and anodization potential. Values shown correspond to an oxalic acid concentration of 0.4 M.

Fig. 4 shows a response surface plot for the oxide thickness. Fig. 4 reports thickness data in terms of a ratio that permits assessment of the efficiency of film formation. The oxidation efficiency, R, is defined as

$$R = \frac{O}{I - M},$$

where O represents the thickness of each oxide layer, I represents half the initial thickness of the aluminum shim, and M represents half the thickness of the metal remaining beneath the film. I and M are halved thickness values so that we consider only the film grown on one side of the aluminum shim. The ratio R can be greater than unity in certain cases due to the lower overall density of the porous oxide film compared to the aluminum substrate. Such cases represent a high anodization current efficiency with respect to oxide formation current, and we therefore sought to maximize R. Achieving a high anodization current efficiency is important to help avoid possible significant decreases in reactor feature size due to excessive aluminum dissolution. In addition, a high anodization current efficiency promotes the conservation of aluminum metal in the "core" beneath the oxide layer, which allows for improved heat transfer throughout the reactor.

Like pore density, the anodization efficiency responded significantly to anodization potential. Unlike pore density, however, which responded to oxalic acid concentration but not temperature, the thickness ratio responded to temperature but not oxalic acid concentration. Thus, the response surface for R could still be represented in two-dimensional form with temperature replacing oxalic acid concentration. Fig. 4 illustrates this surface at the intermediate acid concentration (0.4 M). The surface has the form of a hyperbolic paraboloid. This form confirms several known principles [20–22] of the anodization process. First, as electrolyte temperature increases, the rate of film formation increases for any anodization potential. However, temperatures that are too high also lead to a reduction in current efficiency for oxide formation by increasing the rate of aluminum oxide dissolution into the acid electrolyte, reducing the final film thickness ratio. Also, higher potentials yield correspondingly higher current densities, but these higher currents can cause local temperature gradients across the film surface, leading again to reduced current efficiency for the formation of the oxide.

We sought to obtain the highest anodization efficiency possible, so Fig. 4 suggests the selection of the lowest anodization potential (30 V), which fortunately is consistent with the requirements demanded by pore density. Fig. 4 also suggests a temperature of 18 °C; pore density was insensitive to this parameter. Pore density demanded use of 0.6 M oxalic acid concentration, but the thickness ratio does not depend on this parameter. In summary, the best set of anodization conditions for pore density and thickness ratio is 30 V anodization potential, 0.6 M oxalic acid concentration, and 18 °C electrolyte temperature. These conditions we used for all following anodizations.

4.2. Hydrothermal–thermal treatment

Subjecting microreactors anodized using the optimized conditions described above to hydrothermal–thermal treatments had a significant effect on the total available surface area. Fig. 5 shows that untreated anodized reactors had an average total surface area of about 2.5 m^2. After one hydrothermal–thermal treatment, this area increased dramatically to about 25 m^2. Further treatments caused a gradual decrease, however.

To better explain the trend observed here, consider the surface morphology of the treated oxide films (Fig. 6). Gradually, as the number of treatments increases, the pore structure of the anodic film disintegrates. All that remains after six successive hydrothermal treatments is a sheet of microcrystalline alumina similar to that obtained by sol–gel processes. In contrast to sol–gel processing, X-ray diffraction analysis of the present oxide did not reveal a dominant alumina crystal phase (δ, γ, etc.). This observation may be due to inadequate sample size or interference from the aluminum metal substrate.

4.3. Microreactor kinetics

Table 1 shows how important physical and kinetic characteristics of the catalysts in each microreactor vary with the number of hydrothermal–thermal treatments. Figs. 7–9 show related data for the conversion. For each catalyst,

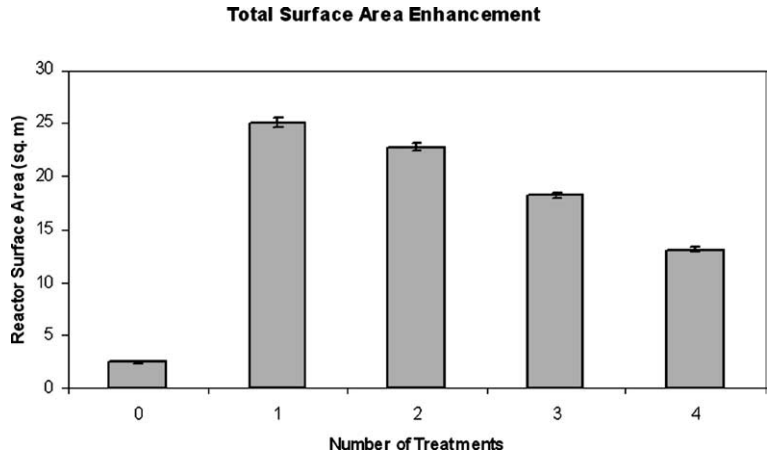

Fig. 5. Total surface area of anodized microreactors after various hydrothermal–thermal treatment cycles.

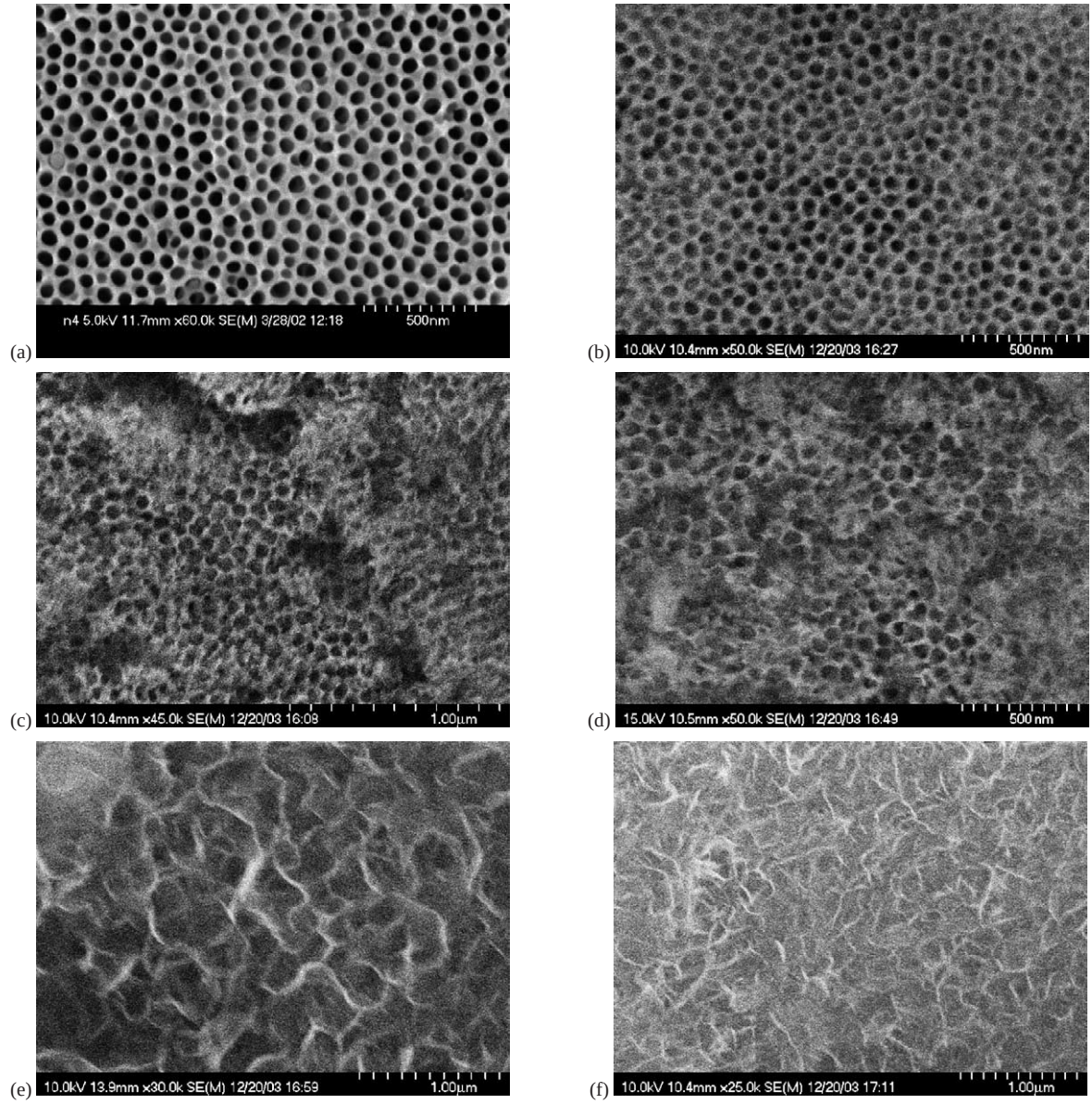

Fig. 6. Surface morphology of anodized microreactors following (a) zero, (b) one, (c) two, (d) three, (e) four, and (f) five hydrothermal–thermal treatments.

Table 1
Catalytic microreactor characteristics

Catalyst	Hydrothermal–thermal treatments	Catalyst dispersion	E_a (kcal/mol)
Ru	0	14%	8.2
Ru	1	23%	8.2
Rh	0	38%	8.4
Rh	1	45%	8.4
Ni	0	8%	13.5
Ni	1	22%	12.0

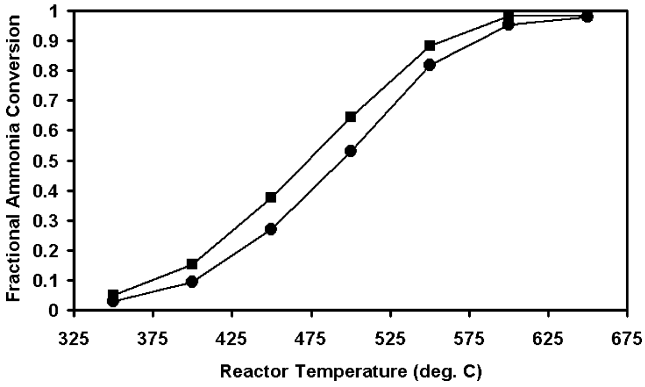

Fig. 7. Fractional conversion of 92 sccm anhydrous ammonia over Ru-catalyzed microreactors following (●) zero and (■) one hydrothermal–thermal treatment.

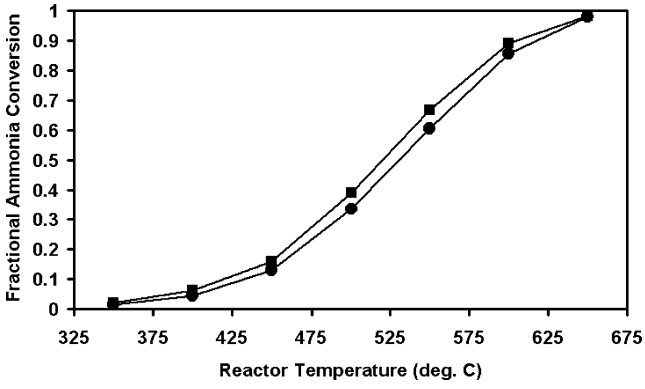

Fig. 8. Fractional conversion of 92 sccm anhydrous ammonia over Rh-catalyzed microreactors following (●) zero and (■) one hydrothermal–thermal treatment.

hydrothermal–thermal treatment slightly increased the dispersion. Rh catalysts exhibited the highest dispersions (38 and 45%), while Ni catalysts showed the largest increase in dispersion as a result of treatment (8 to 22%). Reactant conversions increased in response to treatment for all catalysts, probably due to the increases in both the dispersion and the total surface area of the supporting oxide.

Figs. 10 and 11 show turnover frequencies derived from the conversion and dispersion data for the various catalysts. Table 1 shows the activation energies (E_a) derived from the low-temperature data in these figures, where the rates are limited by catalyst activity rather than by gas-phase transport. Thermal–hydrothermal treatment did not significantly

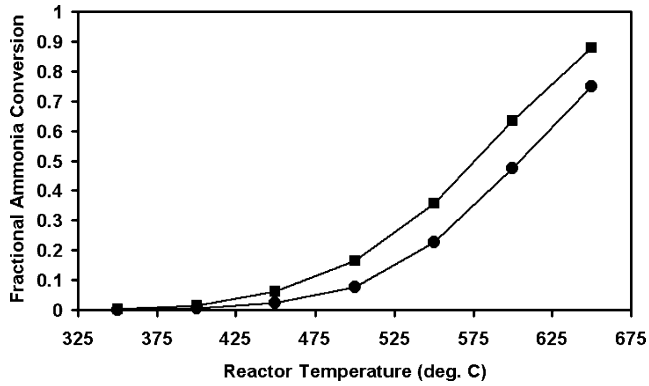

Fig. 9. Fractional conversion of 92 sccm anhydrous ammonia over Ni-catalyzed microreactors following (●) zero and (■) one hydrothermal–thermal treatment.

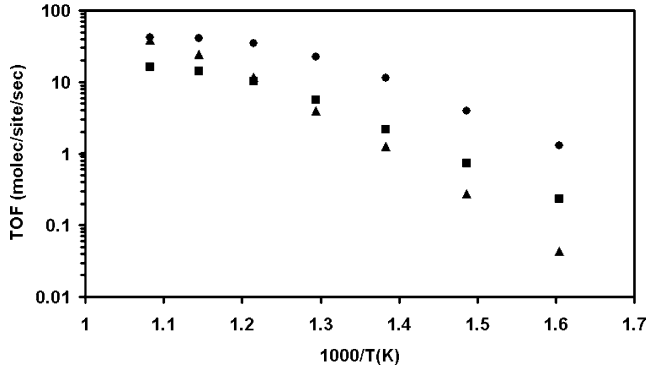

Fig. 10. Turnover frequencies of ammonia decomposition over (●) Ru, (■) Rh, and (▲) Ni catalysts on microreactors with no hydrothermal–thermal treatment, plotted in Arrhenius form.

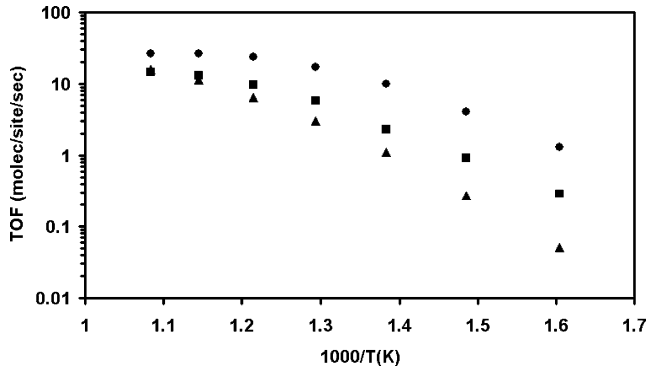

Fig. 11. Turnover frequencies of ammonia decomposition over (●) Ru, (■) Rh, and (▲) Ni catalysts on microreactors with one hydrothermal–thermal treatment, plotted in Arrhenius form.

affect the activation energies, thereby supporting the notion that treatment altered only the availability of metal atoms rather than something intrinsic to the reactions themselves. The magnitudes of the activation energies reported here are comparable to those reported for ammonia decomposition on supported catalysts at conditions near atmospheric pressure [33,34].

5. Conclusions

The results presented here illustrate the effective application of anodic alumina films as catalyst supports in monolithic microreactors constructed from aluminum alloy. The films magnify the original metal surface area up to three orders of magnitude, and up to four orders of magnitude when a hydrothermal–thermal treatment of the film is employed after anodization. The films adhere well to the aluminum substrate and serve as an effective catalyst support capable of dispersing transition metal catalysts to a reasonable extent. Furthermore, we have demonstrated the performance of aluminum–alumina microreactors with optimized porous anodic films for the decomposition of anhydrous ammonia using supported metal catalysts. Microreactors of this type could be used for a variety of heterogeneously catalyzed reactions carried out on a small scale, especially in mobile applications where monolithic structures are advantageous.

Acknowledgments

This work was supported by the Department of Defense Multidisciplinary University Research Initiative (MURI) program administered by the Army Research Office under Contract DAAD19-01-1-0582. Any opinions, findings, and conclusions or recommendations expressed in this publication are those of the authors and do not necessarily reflect the views of the Department of Defense or the Army Research Office.

References

[1] H. Masuda, K. Fukuda, Science 268 (1995) 1466.
[2] O. Jessensky, F. Muller, U. Gösele, J. Electrochem. Soc. 145 (1998) 3735.
[3] D. Almawlawi, K. Bosnick, A. Osika, M. Moskovits, Adv. Mater. 12 (2000) 1252.
[4] Z. Zhang, D. Gekhtmann, M. Dresselhaus, J. Ying, Chem. Mater. 11 (1999) 1659.
[5] Z. Wang, M. Kuok, S. Ng, H. Fan, D. Lockwood, K. Nielsch, R. Wehrspohn, Mater. Phys. Mechan. 4 (2001) 22.
[6] T. Gao, G. Meng, J. Zhang, Y. Wang, C. Liang, J. Fan, L. Zhang, Appl. Phys. A 73 (2001) 251.
[7] J. Li, C. Papadopoulos, M. Xu, M. Moskovits, Appl. Phys. Lett. 10 (1998) 260.
[8] G. Che, B. Lakshmi, E. Fisher, C. Martin, Nature 393 (1998) 346.
[9] A. Michailowski, D. Almawlawi, G. Cheng, Chem. Phys. Lett. 349 (2001) 1.
[10] D. Gong, C. Grimes, O. Varghese, W. Hu, R. Singh, Z. Chen, E. Dickey, J. Mater. Res. 16 (2001) 3331.
[11] S. Ihm, E. Ruckenstein, Ind. Eng. Chem. Process Design Dev. 17 (1978) 100.
[12] G. Patermarakis, C. Pavlidou, J. Catal. 147 (1994) 140.
[13] G. Wiessmeier, D. Hönicke, J. Micromechan. Microeng. 6 (1996) 285.
[14] G. Patermarakis, N. Nicolopoulos, J. Catal. 187 (1999) 311.
[15] G. Patermarakis, H. Karayannis, Electrochim. Acta 40 (1995) 2647.
[16] T. Xu, R. Piner, R. Ruoff, Langmuir 19 (2003) 1443.
[17] X. Zhou, G. Thompson, P. Skeldon, G. Wood, H. Habazaki, K. Shimizu, Corrosion 55 (1999) 561.
[18] G. Alcalá, P. Skeldon, G. Thompson, A. Mann, H. Habazaki, K. Shimizu, Nanotechnology 13 (2002) 451.
[19] J.C. Ganley, E.G. Seebauer, R.I. Masel, AIChE J. 50 (2004) 829.
[20] V. Parkhutik, V. Shershulsky, J. Phys. D: Appl. Phys. 25 (1992) 1258.
[21] A. Li, F. Müller, A. Birner, K. Nielsch, U. Gösele, J. Appl. Phys. 84 (1998) 6023.
[22] G. Patermarakis, K. Moussoutzanis, Corrosion Sci. 43 (2001) 1433.
[23] G. Box, D. Behnken, Technometrics 2 (1960) 455.
[24] D. Ludlow, H. Schulz, J. Erjavek, J. Eng. Educ. 84 (1995) 351.
[25] Y. Abdel-Fattah, Biotechnol. Lett. 24 (2002) 1217.
[26] M. Muthukumar, D. Mohan, M. Rajendran, Cement Concrete Composites 25 (2003) 751.
[27] G. Patermarakis, P. Kerassovitou, Electrochim. Acta 37 (1992) 125.
[28] R. Spooner, W. Forsyth, Plating 55 (1968) 336.
[29] K. Wefers, Aluminum 49 (1973) 553.
[30] S. Desset, O. Spalla, P. Lixon, B. Cabane, Colloids Surf. A 196 (2002) 1.
[31] F. Shüth, K. Unger, in: G. Ertl, H. Knözinger, J. Weitkamp (Eds.), Preparation of Solid Catalysts, Wiley, New York, 1999.
[32] G. Patermarakis, K. Moussoutzanis, J. Chandrinos, Appl. Catal. A 180 (1999) 345.
[33] G. Papapolymerou, V. Bontozoglou, J. Mol. Catal. A 120 (1997) 167.
[34] T.V. Choudhary, A.K. Santra, C. Sivadinarayana, B.K. Min, C.-W. Yi, K. Davis, D.W. Goodman, Catal. Lett. 77 (2001) 1.